Two Compact, Wideband, and Decoupled Meander-Line Antennas Based on Metamaterial Concepts

Colan G.M. Ryan, *Student Member, IEEE*, and George V. Eleftheriades, *Fellow, IEEE*

***Abstract*—A two-antenna system employing wideband metamaterial-inspired meander-line antennas with a maximum separation of $\lambda_0/5$ is presented, and a very wide measured -10 dB return-loss bandwidth from 3.3 to 6 GHz is obtained. Orthogonal characteristic modes on the ground plane are excited, and the coupling between the two antennas is kept below -20 dB over the same frequency band.**

***Index Terms*—Meander-line antenna, metamaterial, multiple-input–multiple-output (MIMO), wideband.**

I. Introduction

TRANSMISSION-LINE metamaterials were introduced in 2002 (see, for example, [1] and [2]) and have since been applied to a variety of microwave devices, including filters, couplers, and antennas [3]–[5]. For the last application in particular, metamaterial components have been used to reduce the size of either the antennas themselves or their feed networks. As the authors showed in [6], however, incorporating a metamaterial unit cell into a quarter-wave meander-line antenna yielded two other benefits: a very wide return-loss bandwidth and codirectional currents on the antenna arms leading to higher radiation efficiency. Here, we expand on our earlier work by offering an improved explanation for the operation of the antenna and by extending the concept to create a compact two-antenna system with low coupling over a very wide bandwidth. This latter application is particularly significant for handheld radios since the proposed device avoids detuning effects and offers the possibility of multiple-input–multiple-output (MIMO) communication due to the low correlation between the individual antennas.

Section II describes the geometry of the single metamaterial antenna and briefly compares its performance to that of a conventional meander-line antenna. Section III presents the two-antenna system and gives the measured results, including radiation patterns and radiation efficiency, of the new design. Concluding remarks are made in Section IV.

Manuscript received August 16, 2012; revised September 30, 2012; accepted October 03, 2012. Date of publication October 18, 2012; date of current version November 27, 2012. This work was supported by the Natural Sciences and Engineering Research Council of Canada (NSERC) and Research-in-Motion (RIM).

The authors are with the Edward S. Rogers, Sr. Department of Electrical and Computer Engineering, University of Toronto, Toronto, ON M5S 3G4, Canada (e-mail: colan.ryan@mail.utoronto.ca).

Color versions of one or more of the figures in this letter are available online at http://ieeexplore.ieee.org.

Digital Object Identifier 10.1109/LAWP.2012.2225134

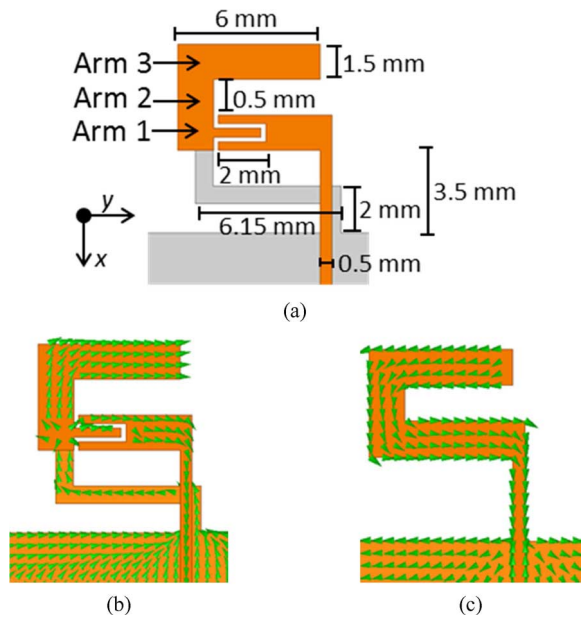

Fig. 1. (a) Geometry of metamaterial-inspired antenna with the ground plane (size: 15×60 mm) colored light gray. (b), (c) Surface current direction on metamaterial-inspired and conventional meander antennas, respectively.

II. Antenna Design

A. Antenna Layout With Metamaterial Unit Cell

Transmission-line metamaterials rely on loading a standard transmission line with a series capacitor and a shunt inductor; the resulting structure possesses a "backward-wave" band where the direction of the phase velocity is reversed with respect to the power flow. The proposed antenna is shown in Fig. 1(a) with the dimensions as indicated. Fed from a microstrip line on a 10-mil (0.254 mm) Rogers RO3003 substrate ($\varepsilon_r = 3$, $\tan\delta = 0.0013$), the antenna incorporates a single metamaterial unit cell on the lower arm: The interdigitated capacitor synthesizes the series capacitance, while the shunt inductor is implemented by the meandered ground plane extension that is connected to the antenna by a via though the substrate. The antenna was simulated in a full-wave simulator, and Fig. 1(b) shows the simulated current flow on the structure at the onset of the operating band at 3.5 GHz. It is observed that in-phase currents are established on both arms. For comparison, a meander-line antenna without the metamaterial unit cell has also been designed and simulated over the same frequency range. Fig. 1(c) shows the direction of the current flow on this "right-handed" antenna, where it is clear that no reversal of

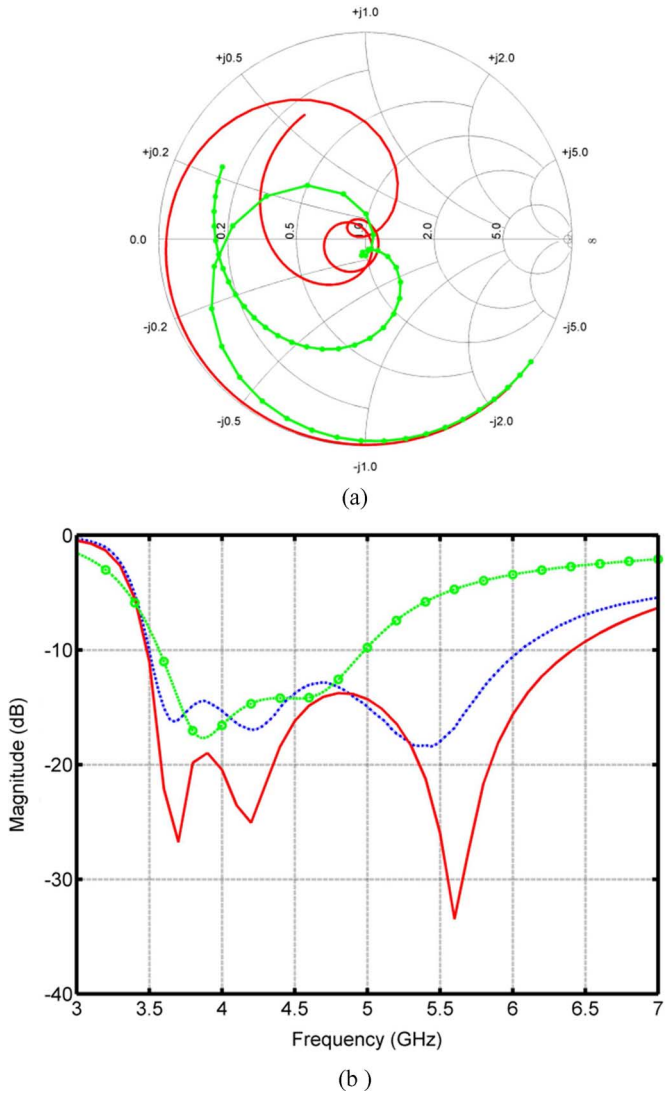

Fig. 2. (a) Smith chart representation of reflection coefficient magnitude for conventional (—●—) and metamaterial (▬) antenna. (b) Cartesian plot of S_{11} magnitude for simulated conventional (—●—) and metamaterial (▬) antenna and for measured metamaterial antenna (■ ■ ■).

the current direction occurs, and so the currents on each of the arms remain out-of-phase. Although this single-cell design does not fully qualify the antenna as a "metamaterial" one, the principle could be applied to a meander-line antenna with many bends; this latter device, in the conventional case, would suffer from reduced radiation efficiency, but applying metamaterial components to each arm would result in all the arms radiating in-phase, thereby increasing efficiency, radiation resistance, and bandwidth.

B. Comparison of Conventional and Metamaterial Meander Antennas

Another benefit of the new antenna is its wider bandwidth as compared to the conventional meander as shown in Fig. 2. The Smith chart of Fig. 2(a) shows that a second loop appears in the S_{11} response of the new metamaterial-inspired antenna and a significantly wider bandwidth is obtained. In Fig. 2(b), the -10 dB bandwidth extends from 3.5 to 6.5 GHz, whereas the

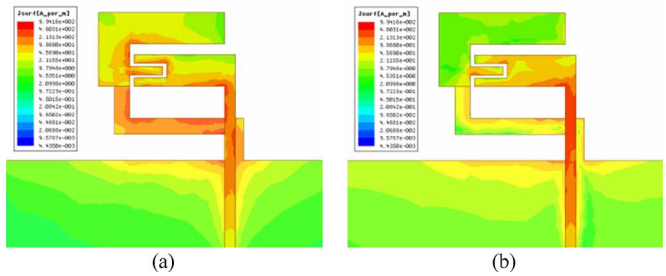

Fig. 3. Simulated current magnitude at (a) 4 and (b) 5.6 GHz.

conventional meander antenna has a -10 dB bandwidth from 3.6 to 5 GHz. This extra resonance arises since the ground trace now forms a second resonant length in addition to that of the antenna itself. Fig. 3(a) and (b) plots the magnitude of the surface current as simulated in HFSS at 4 and 5.6 GHz, respectively. It is seen that current flows over the entire antenna at the lower frequency, but is confined to the first arm and the ground extension at the upper band. With its improved impedance match, the proposed antenna may look similar to a monopole with an embedded "gamma-match" circuit [7]. However, this approach does not result in the aforementioned in-phase currents.

C. Measured Results for Single Antenna

The measured return loss is also shown in Fig. 2(b). The total measured -10 dB return-loss bandwidth is 2.5 GHz, and reasonably good agreement between the two sets of data is obtained. The discrepancy in overall magnitude between measured and simulated results is due to the relatively large radius of the coaxial feeding pin; simulations confirm a degradation of matching levels when the inductance of the feed line is decreased as the line itself is widened. The radiation patterns are very similar to those obtained for the two-antenna system, which will be shown in the following section and so are not repeated here. The radiation efficiency was calculated using McKinzie's Wheeler cap method [8] and was above 87% across the band.

III. Two-Antenna System With Low Mutual Coupling

A. Introduction

Given the excellent single-antenna results, a two-antenna system with a small size was sought in which low mutual coupling could be obtained while yet preserving the wideband individual return-loss characteristics already described. Such a device would have several advantages: First, due to the decoupling, multiple antennas could occupy a smaller space with little impact on their individual performance; second, these antennas could have potential uses in MIMO technology. In this latter role, a low coupling, (described here using the *S-parameters* transmission gain S_{21}) can be related to the envelope correlation coefficient between two antennas [9]. Low coupling, and hence low correlation, implies the channels seen by the individual antennas are independent, thus leading to higher overall data rates [10]. Since measuring the actual data throughput is beyond the scope of this paper, we confine ourselves to making *S-parameter* measurements and to demonstrating low antenna coupling.

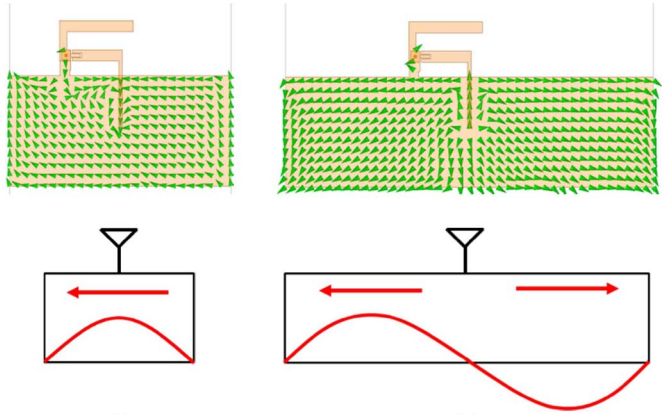

Fig. 4. Ground plane surface current plots and schematics at 4 GHz for ground plane widths of (a) 30 and (b) 50 mm.

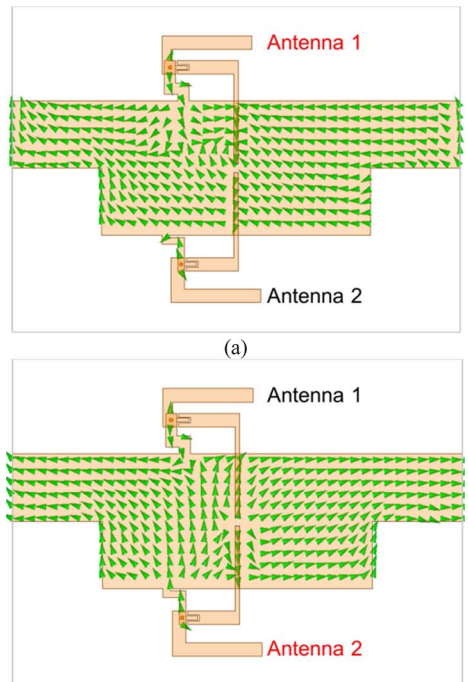

Fig. 5. Simulated surface current distribution on modified ground plane showing (a) Antenna 1 (on top) exciting the half-wave mode and (b) Antenna 2 (on bottom) exciting the full-wave mode.

B. Exciting Two Characteristic Modes on the Ground Plane

To obtain two decoupled antennas, two orthogonal modes on the ground plane were excited, and they are shown in Fig. 4 for two different ground plane sizes at the same frequency. In Fig. 4(a), the ground plane is electrically smaller, and consequently, a "half-wave" mode is excited; when the ground becomes larger, a "full-wave" resonance is supported. Corresponding to the characteristic modes of the ground plane [11], these two current distributions are orthogonal and so would theoretically have a coupling value of zero. Since it is not possible to dynamically change the size of the ground plane, the novel approach reported here is to combine both ground shapes into one, as illustrated in Fig. 5. The intent was to allow each antenna to excite different modes on different areas of the ground, and various configurations (including tapering the transition between the two ground regions) were investigated. The figure shows the optimal geometry. This figure also shows that at a frequency of 4 GHz, either a half-wave or full-wave mode is excited depending on which antenna is active. Consequently, low coupling between the antennas can be achieved.

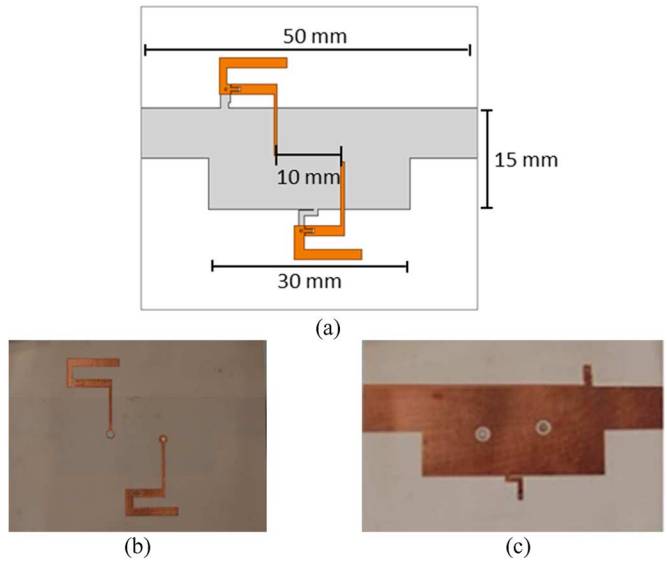

Fig. 6. (a) Dimensions of final device, and photographs of fabricated antennas for (b) top layer and (c) bottom layer.

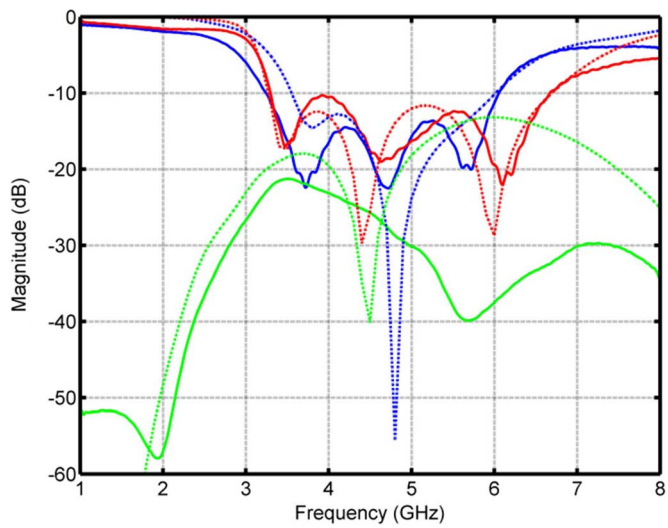

Fig. 7. Measured (solid lines) and simulated (dotted lines) *S-parameters* for two-antenna system: S_{11} (—), S_{22} (—), S_{21} (—).

C. Simulated and Measured Results

The two-antenna system, shown in Fig. 6, was fabricated on the same substrate mentioned previously. To accommodate the feed cables, the antennas had to be moved farther apart than in initial simulations and were separated by 10 mm, which corresponds to $\lambda_0/5$ at the highest frequency. The simulated and measured *S-parameters* are shown in Fig. 7. Overall, good agreement is obtained between the two sets of data. A very wide measured return-loss bandwidth from approximately 3.3–6 GHz is achieved, and the coupling between the two

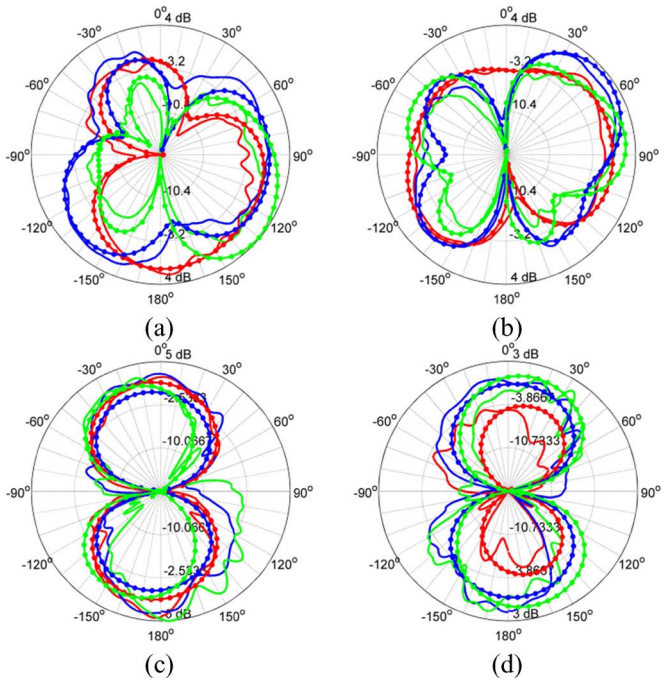

Fig. 8. Measured (solid lines) and simulated (marked lines) radiation patterns at 3.5 GHz (▬), 4.5 GHz (▬), and 5.5 GHz (▬). (a), (b) Gain φ in xy-plane for antennas 1 and 2. (c), (d) Gain θ in xz-plane for antennas 1 and 2.

TABLE I
MEASURED AND SIMULATED RADIATION EFFICIENCY OF TWO-ANTENNA SYSTEM

Frequency (GHz)	Antenna 1 η_{RAD}		Antenna 2 η_{RAD}	
	Meas.	Sim.	Meas.	Sim.
3.5	79%	94%	84%	95%
4.6	78%	98%	80.5%	98%
5.8	86%	99%	79%	99%

antennas never exceeds -20 dB over that interval. Perhaps as a result of the nonideal coaxial feeds connectors soldered onto the ground plane (and thereby affecting the ground plane current distribution), the coupling performance is actually better than that predicted by simulation. It is interesting to note that in simulation the coupling levels remain approximately the same even as the antenna spacing decreases to the case shown in Fig. 5. Fig. 8 compares the measured and simulated radiation patterns for each individual antenna where roughly omnidirectional patterns are obtained. The greatest discrepancy occurs in the backlobe of the E-plane of the antennas and is due to radiation from both the feed cable and the 50 Ω load used to terminate the nonfed antenna that was not completely suppressed. Overall, however, the behavior of the fabricated device shows very good agreement with its simulated counterpart. Finally, Table I gives the radiation efficiencies for each antenna. Although lower than those predicted by simulations (which use ideal feeding ports), the measured values range from 79% to 85% across the band and demonstrate good performance.

IV. CONCLUSION

Metamaterial meander-line antennas have been used to create a two-antenna system that has a very wide 2.7 GHz return-loss bandwidth and low -20 dB coupling despite having a maximum separation of only $\lambda_0/5$. The metamaterial loading on each individual antenna results in codirected currents and introduces a second resonance that increases bandwidth; the novel ground plane shape allows for two orthogonal characteristic modes to be excited, thus leading to excellent isolation. Good agreement between simulated and measured performance was noted. The combination of small size, good matching, high decoupling, and high radiation efficiency makes this new design well suited for use in next-generation mobile handset radios.

REFERENCES

[1] G. V. Eleftheriades, A. K. Iyer, and P. C. Kremer, "Planar negative refractive index media using periodically L-C loaded transmission lines," *IEEE Trans. Microw. Theory Tech.*, vol. 50, no. 12, pp. 2702–2712, Dec. 2002.

[2] C. Caloz and T. Itoh, *Electromagnetic Metamaterials: Transmission Line Theory and Microwave Applications*. Hoboken, NJ: Wiley, 2006.

[3] M. Duran-Sindreu, G. Siso, J. Bonache, and F. Martin, "Planar multiband microwave components based on the generalised composite right/left handed transmission line concept," *IEEE Trans. Microw. Theory Tech.*, vol. 58, no. 12, pp. 3882–3891, Dec. 2010.

[4] F. Qureshi, M. A. Antoniades, and G. V. Eleftheriades, "A compact and low-profile metamaterial ring antenna with vertical polarization," *IEEE Antennas Wireless Propag. Lett.*, vol. 4, pp. 333–336, 2005.

[5] C.-J. Lee, K. M. K. H. Leong, and T. Itoh, "Composite right/left-handed transmission line based compact resonant antennas for RF module integration," *IEEE Trans. Antennas Propag.*, vol. 54, no. 8, pp. 2283–2291, Aug. 2006.

[6] C. G. M. Ryan and G. V. Eleftheriades, "A wideband metamaterial meander-line antenna," in *Proc. 6th Eur. Conf. Antennas Propag.*, Prague, Czech Republic, Mar. 26–30, 2012, pp. 2329–2331.

[7] C. R. Rowell and R. D. Murch, "A capacitively loaded PIFA for compact mobile telephone handsets," *IEEE Trans. Antennas Propag.*, vol. 45, no. 5, pp. 837–842, May 1997.

[8] W. E. McKinzie, III, "A modified wheeler cap method for measuring antenna efficiency," in *Proc. IEEE Int. Symp. Antennas Propag.*, Montreal, Canada, Jul. 1997, pp. 542–545.

[9] J.-F. Li and Q.-X. Chu, "Proximity-fed MIMO antenna with two printed IFAs and a wideband T-shaped neutralization line," *Prog. Electromagn. Res. M*, vol. 21, pp. 279–294, 2011.

[10] Q. Wang, H. Zhang, D. Plettemeier, E. Ohlmed, and G. Fettweis, "Design and performance evaluation of handset MIMO antenna prototypes," in *Proc. Int. Workshop Smart Antennas*, 2010, pp. 375–382.

[11] M. Cabedo-Fabrés, E. Antonino-Daviu, A. Valero-Nogueria, and M. Bataller, "The theory of characteristic modes revisited: a contribution to the design of antennas for modern applications," *IEEE Antennas Propag. Mag.*, vol. 49, no. 5, pp. 52–68, Oct. 2007.